Published in final edited form as:
Nat Methods. 2019 October ; 16(10): 994–997. doi:10.1038/s41592-019-0572-y.

4D functional ultrasound imaging of whole-brain activity in rodents

Claire Rabut[1], **Mafalda Correia**[1], **Victor Finel**[1], **Sophie Pezet**[1], **Mathieu Pernot**[1], **Thomas Deffieux**[1,+], **Mickael Tanter**[1,+]

[1]Physics for Medicine, Inserm U1273, ESPCI Paris, PSL Research University, CNRS FRE 2031, Paris, France

Abstract

We developed a technology that extends the capabilities of functional ultrasound to whole-brain 4D neuroimaging. We implemented multiplane wave transmissions on matrix arrays at thousands of frames per second to provide volumetric recordings of cerebral blood volume changes at high spatiotemporal resolution. This approach is illustrated by several proofs-of-concept: real time multiple sensory stimuli, 4D functional connectivity and instantaneous tracking of epileptiform events within the whole brains of rodents.

Functional neuroimaging has become an invaluable tool in neurosciences, especially to study the brain as a dynamic global network of interacting regions. Typical neuroimaging modalities such as magnetic resonance imaging (MRI), electroencephalogram, magnetoencephalography offer a wide field of view at the price of either a limited spatio-temporal resolution or sensitivity[1]. Conversely, electrophysiology or optical techniques offer very high spatio-temporal resolutions but in a limited field of view. As of today we have a fragmented understanding of the brain as a large-scale network. Long acquisition times at high frame rates are essential to monitor spontaneous neuronal activities. Moreover, to fully understand the brain activity, imaging with a large field of view is capital. Photoacoustics tomography could emerge as such an interesting modality and has shown promising results

*MT is corresponding author: mickael.tanter@gmail.com.
+T.D. and M. T. are co-last authors.

Data availability

All data supporting the findings of this study associated with figures are available upon request. Example data can be downloaded in the supplementary materials of the publications on the Nature Methods website.

Code availability

Example encoding and postprocessing codes associated with figures can be downloaded in the supplementary materials of the publications on the Nature Methods website. Step-by-step instructions are available in a Readme pdf document to guide the user. A binary executable file for GPU-based 3D beamforming is included to process decoded sample RF data. The low level beamforming code is available in the framework of an official collaboration between academic institutions.

Author Contributions

M.T. and T.D. conceived the study. C.R, V.F., M.P. and M.C. developed sequence acquisitions, C.R. and S.P. acquired data. C.R., T.D. and M.T. performed data processing. C.R., S.P., T.D. and M.T. interpreted the results. C.R. and M.T. wrote the first draft of the manuscript with substantial contribution from T.D., S.P. and M.P. All authors edited and approved the final version of the manuscript.

Competing Financial Interests

T.D., M.P. and M.T are co-founders and shareholders of Iconeus company commercializing ultrasound neuroimaging scanners.

Europe PMC Funders Author Manuscripts

on rodents[2,3,4] where the penetration depth limited by the acceptable light fluence safety exposure is less critical.

Functional UltraSound (fUS) imaging provides an alternative and portable method to image dynamic deep brain activation by directly measuring subtle cerebral blood volume (CBV) changes[5,6] induced by neurovascular coupling[7]. Its spatio-temporal resolution and sensitivity offer a compelling tool to study dynamic activation patterns in a large field of view. fUS imaging relies on plane wave transmissions and highly parallel electronics[8] to achieve ultrafast framerates (>5,000 frames/s) and reach ultrasensitive Doppler imaging. This neuroimaging modality is currently limited to acquisitions in a 2D imaging plane, as ultrasensitive Doppler relies on a limited number of channels and was only able, until recently, to drive 1D ultrasonic linear probes.

However, following spontaneous or transient activation patterns or measuring functional connectivity (FC) between remote structures requires the simultaneous acquisition of information in the whole brain.

Although 2D piezoelectric matrix array transducers have started to emerge for volumetric imaging applications, those remain hampered by major bottlenecks, such as a low individual element sensitivity compared to conventional 1D linear probes, or integrated sequential pre-beamforming required to lower data transfer rate from the probe to the scanner. These issues become critical for applications that require both ultrafast frame rates and high sensitivity such as in fUS neuroimaging.

Here, we propose an innovative methodology to circumvent these different issues and extend ultrasound neuroimaging to 4D (3D:space + 1D:time) whole brain fUS imaging. Our approach relies on the design of a high frequency 2D matrix array transducer technology (8MHz, 0.3mm-pitch, Vermon, France) coupled with a high channel count electronic system for ultrafast 3D imaging. To counterbalance the poor sensitivity of matrix elements, volumetric acquisitions at ultrafast frame rates (thousands of volumes per second) are obtained following an innovative 3D multiplane wave scheme with 3D spatiotemporal encoding of transmit signals using Hadamard coefficients[9]. For each transmission, the backscattered signals containing mixed echoes from the different plane waves are decoded using the synthetic summation of echoes from successive receptions with appropriate Hadamard coefficients. This enables the retrieval of echoes from a virtual individual plane wave transmission with an N-fold higher amplitude (Fig 1a). Finally, coherent compounding beamforming of decoded echoes is performed to produce 3D ultrasonic images and a spatiotemporal clutter filter separating blood flow from tissue motion is applied to compute a power Doppler volume (proportional to the CBV).

While functional ultrasound imaging can be performed through the intact skull in mice[7] or with contrast agents through the intact skull in rats[10], we performed here a craniotomy surgery to prepare the animals for imaging. Whole-brain ultrasensitive Power Doppler volumes (proportional to CBV) were acquired using the 3D multiplane wave sequence at almost 400 compounded volumes per second. Major arteries of the rat brain such as the superior sagittal sinus (sss) as well as the Willis circle (pcer), located at 6 mm depth, as well

as smaller vessels, particularly in the cortex, were clearly visible in the reconstructed 3D volume with a 170*170*85 μm^3 voxel size (Fig 1b).

We then validated 4D fUS imaging in three tailored applications in the rat brain. We first present sensory-evoked activations using either visual or whisker stimulations (Fig. 1b-c and Supplementary Video 1). Second, 3D FC between remote brain structures is estimated during rest using seed-based and correlation matrix analysis (Fig. 2a-b-c and Supplementary Fig. 1). Finally, 4D fUS is shown to map in detail the whole-brain propagation of transient epileptiform events (Figure 2d and Supplementary Video 2).

During ad-hoc whiskers stimulations and then of the visual system using a flashing LED, power Doppler images were acquired and the temporal evolution of CBV in each pixel was correlated to the stimuli patterns to generate 3D correlation maps (Fig. 1b-c and Supplementary Video 1). In N=3 rats, whiskers and visual stimulations induced a robust activation maps in several brain areas (Fig. 1).

In a second experiment, we considered spontaneous low-frequency (0.05 to 0.3Hz) brain fluctuations observed in 2D fUS[11] and fMRI[12] in N=4 rats. Using seed-based analysis, we observed that both right and left hippocampus signals were highly correlated (r=0.7) (Fig. 2a). This result is in agreement with extensive literature showing strong anatomically and functionally[13] links between hippocampus, but also bilateral cortical links, due to cortico-cortical projections. Leveraging fUS imaging to whole-brain 4D acquisitions expands the size of FC matrices in rodents by one order of magnitude compared to recent results[11].

We then analyzed the pair-wise correlations between hundreds of regions of interest to construct a FC matrix. Similarly to fMRI[12], clusters of synchronized activity corresponding to large brain regions can be observed – revealed by squares in the matrix - as well as strong bilateral connections – revealed by anti-diagonals in the matrix (Fig. 2b-c). The inter-animal reproducibility of these connectivity maps was very satisfactory for all N=4 animals (Supplementary Fig. 1).

Finally, to demonstrate the acquisition capabilities of 4D fUS imaging for whole brain tracking of transient and complex phenomena, we induced epileptiform events using a 4AP injection in the cerebral cortex of N=3 rats and imaged their dynamic propagation through the whole-brain. Mapping relative CBV variations, cortical spreading depression waves propagated from the point of injection toward the contralateral cortex and in deeper laminae of the ipsilateral cortex (Fig. 2d and Supplementary Video 2). Using isochronous maps (Supplementary Fig. 2 and Supplementary Video 3), the propagation speed was measured at 3 +/-0.3 mm/min, which is in agreement with previous studies in rabbits[14] and rats[15]. Propagation of ipsi and contralateral spreading depressions were detected in two animals among N=3 animals (Supplementary Fig. 3).

We hereby demonstrated for the first time that 4D fUS imaging can be used for dynamic whole-brain functional imaging on rodent models.

As any other neuroimaging modality, fUS imaging also has limitations. First, fUS is sensitive to CBV variations and as such is measuring brain activity only through the prism of

Europe PMC Funders Author Manuscripts

the neurovascular coupling. Although fUS is limited by the inherent delay of the neurovascular coupling, its 20ms temporal resolution could be taken benefit from to map the directional propagation of vascular activity based on lag-correlation mapping as recently demonstrated in behaving non-human primates during visual tasks[16].

Secondly, compared to Photoacoustics or fMRI, it does not give access to the valuable oxygen saturation information. For this reason, it does not measure an initial dip in the functional response to stimuli. fUS is also blind to quasi-horizontal vessels which could also contain valuable information. Thirdly, the current spatial resolution, estimated at 240x240x180microns in the center of the imaged volume and 320x320x180microns on the volume edges (Figure S4) is lower than for 2D fUS imaging. It could be further improved by using a refined one-wavelength pitch or, increasing frequency up to 15MHz. Fourth, our setup still requires a craniotomy for rat brain imaging or the intravenous injection of microbubble contrast agents to become non invasive[10]. Fifth, compared to optical approaches, fUS imaging is not able to provide voltage/calcium ultrasonic indicators but the emergence of nanometric genetically encoded gas vesicles as acoustic reporter genes could pave the way to such indicators in the future[17]. Finally, although one great advantage of 2D fUS imaging is that the probes are small enough to be used with awake freely moving animals[18], here, due to the large number of cables and weight of the array, it is not possible to date to use 4D fUS directly in such condition but only in head-fixed animals.

The recent clinical demonstrations of the 2D fUS technique could also directly benefit from our 4D strategy both non-invasively in human neonates through the trans-fontanellar window[19] and in adults during surgery. 4D clinical fUS imaging would then provide whole functional data in a short time span without the need for a careful positioning of the probe prior to acquisition. For fundamental research, 4D fUS imaging in combination with other modalities such as electrophysiology or optogenetics could strongly extends our capabilities of whole brain observation in small animal imaging.

Online Methods

Animal preparation

All animals received humane care in compliance with the European Communities Council Directive of 2010 (2010/63/EU), and the study was approved by the institutional and regional committees for animal care: CEEA (Comité d'Ethique pour l'Expérimentation Animale) numéro 59 - "Paris Centre et Sud" Protocole # 2017-23).

Sprague Dawley male rats were used in this study (6-8 weeks old, 250-350g). N=10 animals were used for this study. 4D fUS imaging with visual and/or whisker stimuli was performed N=3 animals. Imaging of ictal events was performed in N=3 rats. 3D functional connectivity mapping was performed in N=4 rats.

A craniotomy was performed to avoid the effect of the skull, which can produce significant attenuation and distortion of ultrasound signals at the employed frequencies.

During the surgery and the subsequent imaging session, the animals were anaesthetized using an initial IP injection of medetomidine (Domitor®, 0.3 mg kg^{-1}) and ketamine (Imalgene®, 40 mg kg^{-1}), followed by hourly IP injections of medetomidine (Domitor®, 0.1 $mg.kg^{-1}.hr^{-1}$) and ketamine (Imalgene®, 12.5 $mg.kg^{-1}.hr^{-1}$). The animal head was placed in a stereotaxic frame and a 1x1 cm skull window was removed by drilling (Foredom, USA) at low speed using a micro drill steel burr (Burr number 19007-07, Fine Science Tools, Vancouver, Canada). Care was taken not to damage the dura to prevent inflammatory processes in the brain.

After surgery, the brain was rinsed with sterile saline, and ultrasound coupling gel was placed on the window. The 2D matrix array was positioned directly above the cranial window prior to acquisition.

During both the craniotomy and the imaging session, the body temperature was maintained constant using a heating pad (Physitemp), and heart and respiratory rates were monitored (MouseOx plus, Starr Life Science corp.). The eyes of the animal were covered with black masking tape during the surgery so that the light from the scialytic lamp would not saturate the ocular receptors of the animals and produce visual stimulation.

3D ultrafast system with multiplane wave encoding

A 3D ultrafast scanner[20] (1024/512 transmit/receive channels, 60 MHz sampling rate) was used to drive a 32-by-32 piezoelectric matrix array transducer (0.3 mm element size, 8 MHz center frequency, Vermon, Tours, France). Each individual element has a 0.3x0.3 mm^2 size (corresponding to $4\lambda^2$ much smaller than the typical $20\lambda^2$ of conventional linear probes). The system has been used in recent studies with compounded plane wave transmissions to allow 3D ultrafast volumetric acquisition at thousands of volumes per second to perform 3D shear wave elastography in tissue mimicking phantoms.

To reach a mandatory high signal-to-noise ratio for 4D whole-brain fUS imaging, a transmission sequence based on the emission of a burst composed of multiple tilted plane waves with Hadamard amplitude encoding was implemented.

Briefly, multiplane wave imaging (MP) enables an increased signal-to-noise ratio for ultrafast images without compromising either the frame rate or resolution. It also regains the sensitivity loss due to the small element size of the 2D matrix array. This concept was tested for 2D ultrafast imaging[9] but never implemented for 3D imaging.

Multiplane wave imaging relies on coded excitations: each emission transmits a burst of successive N plane waves with different angle transmits with each plane wave having a given coded polarity (-1 or +1). N successive transmits are then fired with the same set of plane waves but different polarity combinations (Supplementary Fig. 5). By using different polarities, one can then reconstruct individual plane waves independently with linear operations on receive buffers using linear formation.

To optimize those polarity combinations for N emissions of the N tilted plane waves p_1, …,p_N, a Hadamard matrix was used to obtain independent vectors with +1 and -1 components from each of its columns. Noting that the multiplication of H_N (N^{th} order

Hadamard matrix) by its transpose is equal to N times the identity matrix I: $H_N . H_N^t = N . I$. Thus, the backscattered echoes of each independent plane wave can be reconstructed individually by a dedicated coherent summation of the successive receive signals.

Finally, by coherently summing the N initial receive buffers of the N successive transmissions with the right coefficients given by the Hadamard matrix lines, we can reconstruct N new buffers corresponding to backscattered echoes of individual plane waves only, but with a virtual amplitude N times greater.

As an example, for N=2, the rows and columns of Hadamard matrix $H_2 = \begin{bmatrix} 1 & 1 \\ 1 & -1 \end{bmatrix}$ are used respectively for the coding and decoding of 2 successive multiplane wave transmissions. The first and second transmissions correspond respectively to the combined emission of p_1+p_2 and p_1-p_2 based on :$H_2 . \begin{pmatrix} p_1 \\ p_2 \end{pmatrix} = \begin{pmatrix} p_1 + p_2 \\ p_1 - p_2 \end{pmatrix}$. By multiplying the resulting backscattered signals by H_2^t ,, one can decode the echoes and synthetically reconstruct the signals virtually transmitted by $2p_1$ and $2p_2$ as $H_2^t . \begin{pmatrix} p_1 + p_2 \\ p_1 - p_2 \end{pmatrix} = H_2^t . H_2 . \begin{pmatrix} p_1 \\ p_2 \end{pmatrix} = \begin{pmatrix} 2p_1 \\ 2p_2 \end{pmatrix}$.

The order of a Hadamard matrix (and thus the number of tilted plane waves) must be 2 or a multiple of 4. In our sequence, we used N=8 plane waves (MP 8-angles transmit sequence) (Table 1 for angles of tilted waves and Supplementary Fig. 5), enabling an important gain ($\sqrt{8}$) of SNR without compromising the frame rate (390 Hz). Using such coded excitations, we managed to achieve high quality Doppler volumes thanks to an artificial increase in the amplitude of the transmit signal. In order to estimate the improvement achieved by multiplane transmit imaging, we performed one multiplane transmit scheme (Sequence A) lasting 350 ms followed by a conventional plane wave compounding sequence with N=8 successive individual compounded plane wave transmissions lasting 350 ms. The 9 dB SNR increase obtained by multiplane wave transmit compared to conventional plane wave compounding permits to image many vessels which were hidden in the conventional compounding sequence (Supplementary Fig. 6).

4D functional ultrasound sequences

Different sequences were implemented for the 4D functional ultrasound experiments:

- Sequence A: *sensory-evoked experiment*

  A Multiplane-Wave 8-angles (MP 8-angles) transmit sequence (3120 Hz transmission rate) is repeated at 390 Hz for 350 ms to average approximatively two cardiac cycles. This enables the construction of 136 compounded ultrafast volumes, which form a Power Doppler volume when squared and averaged.

  Each power Doppler imaging block **is repeated every 1.5 s** (1.15 s pause time) **during 180 s**. Several successive acquisitions were performed in a row and concatenated.

- Sequence B: *functional connectivity experiment*

  The same MP 8-angles transmit sequence in Sequence A (repeated at 390 Hz for 350 ms) is used. Imaging blocks also are **repeated every 1.5 s** (1.15 s dead time) **for 300 s**. This long acquisition time is adapted to measure functional connectivity.

- Sequence C: *epileptiform activity experiment*

  The same MP 8-angles transmit sequence in Sequence A (repeated at 390 Hz for 350 ms) is used **but repeated every 3 s** (2.65 s dead time) **for 360 s**.

A pause between imaging blocks as well as sequence repetitions was initially chosen as a compromise between the frame rate (to ensure adequate blood volume variations sampling) and a conservative dead time (needed both for the continuous storage of raw data and to prevent any possible damage of our prototype probe due to any internal accumulated heating). In the future, we expect faster storage units, as well as a less conservative approach toward probe safety to reduce the dead time as much as possible. This would boost temporal sampling to achieve continuous blood volume monitoring, as is currently possible with 2D functional ultrasound imaging.

Beamforming and ultrasensitive Doppler processing

The first step of the beamforming process is the decoding and coherent compounding of raw channel data. As described previously, we first recombined the received data of successive transmits with the coefficients given by the Hadamard matrix. As a result, we obtained, for each sequence of N transmission containing N-angles multiplane waves, N receive buffers after synthetic decoding. Each of them virtually resulted from a single tilted 2D plane wave emission with an N-fold higher amplitude. We then compensated each time delay dt_i, and the resulting N buffers were coherently summed to obtain one final buffer, as in the coherent compounding method[21].

Volume beamforming was then performed using a delay-and-sum processing implemented on a graphical processing unit (K6000, Nvidia, Santa Clara, CA) to reconstruct a volumetric dataset.

The clutter filter then removed all static or quasi-static information corresponding to slowly moving tissue to keep only the signals coming from blood scatters. We implemented a multidimensional spatiotemporal filtering based on a singular value decomposition[22], which was extended to 4D data (time+ 3D space). The algorithm allowed the discrimination of tissue motion (coherent motion within the volume) from blood flow (incoherent motion within the volume) by eliminating the coherent subspace corresponding to the first singular vectors (n= 30) of the data decomposition.

After a clutter filter and for each voxel, the energy of the temporal signal was integrated over the whole imaging block (corresponding to 350 ms) to obtain one ultrasensitive power Doppler volume. The block duration was chosen so that the CBV was averaged over approximately two cardiac cycles to remove the influence of the pulsatility. Power Doppler images have been shown to be quasi proportional to blood volume[5].

In order to estimate the spatial resolution of 4D fUS imaging using the 9 Mhz Matrix array and multiplane wave transmit sequence, we imaged a 80 μm diameter nylon wire in water by applying the 3D decoding and 3D beamforming with an isotropic 85x85x85 voxel size. This static wire was placed at different locations both in depth and lateral directions in order to estimate the spatial resolution in the center and in the periphery of the imaged volume. We found a 240x240x180 μm spatial resolution in the middle of the 3D imaged volume. This spatial resolution was slightly and continuously decreasing towards the lateral borders of the imaged volume up to a 320x320x180 μm value near the corners.

For all the in-vivo data, considering the spatial resolution and the time of beamforming inversely proportional to the size of the reconstructing voxel, we chose to beamform with a 170*170*85 μm^3 voxel. This corresponds to approximately $\lambda*\lambda*\lambda/2$.

Although fUS imaging is able to detect very slow blood flow (1 mm/s) variation occurring in tiny vessels[23], it permits to image only vessels with diameter comparable or higher than the spatial resolution. For this reason, only arterioles or venules with a diameter larger than 100 μm are visible and delineated in fUS images. In the brain cortex such large vessels are mainly perpendicular to the brain surface. Nevertheless, the fUS signal is able also able to image large arterioles and venules with angles ranging between 0° and more than 70° compared to the ultrasonic beam axis as demonstrated in [Mace et al 2013]. As an example, vessels such as the superior sagittal sinus or inferior sagittal sinus are clearly visible in Fig. 1 and Fig. 2.

A guide for implementation, Hadamard coding and decoding and data examples are provided in Supplementary Software package. Step-by step instructions are provided in the Readme pdf document. These data and codes can be downloaded in the supplementary materials of the publication on the Nature Methods website.

Sensory-evoked 3D functional imaging

To highlight the spatio-temporal specificity of the 3D imaging system, we performed (on the same rat) two different stimulations following each other: whisker stimulation and visual stimulation.

Whisker stimulation—the whole (left) pad of whiskers was stimulated manually using a cotton swab using the following parameters: 15 s ON period, 5-7 Hz, 1 cm amplitude, separated by a 15 s OFF period (starting with the OFF period). The stimulation pattern was repeated 6 times for a total acquisition duration of 180 s.

Visual stimulation—Visual stimuli were delivered using a green LED (532 nm wavelength) positioned at 3 cm in front of the right or left eye of rats. At this distance, the light luminance was of 18 lx when the light was ‘ON’ and of 0.01 lx when the light was off. Stimulation runs consisted of periodic flickering of the green LED using the following parameters: 15 s of rest followed by 15 s of a flicker repeated 6 times for a total duration of 180 s. Between stimuli presentation sessions, the rats were kept in a dark environment.

Europe PMC Funders Author Manuscripts

Activation maps

Correlation maps were computed individually from the normalized correlation between each voxel temporal signal with the different stimulus patterns (Pearson's product moment) using MATLAB (MathWorks, Cambridge, MA, USA). Example Matlab codes for all post-processing steps are included in Supplementary Software.

We chose a level of significance of $z > 3.1$ by applying the Fisher's transform ($P < 0.001$, one tailed test), which corresponds to $r > 0.193$. The map after thresholding for the same example is shown in figure 1b. Brain structures (S1BF, VPM) were identified using a rat brain atlas by performing a rigid registration of the corresponding coronal slice.

Ultrasensitive Doppler volumes, relative cerebral blood volume and correlation volumes were then imported in a 3D software for visualization (Amira 6.0.1 software, Visualization Sciences Group, Burlington, MA).

3D functional connectivity matrix

Functional ultrasound has been shown to reveal intrinsic brain connectivity patterns in the rat[11]. We followed here the same protocol and anesthesia: namely keeping the animal under medetomidine (Domitor®, 0.3 mg kg^{-1}) and ketamine (Imalgene®, 40 mg kg^{-1}) for at least 2 hours before the acquisition to obtain stable and reproducible results.

Eight acquisitions of 90s each were acquired and then concatenated. Datasets were filtered independently with a high-pass filter with a cutoff frequency of 0.05 Hz.

Functional Connectivity was studied through the lens of two analysis—We first selected two seeds located in the left hippocampus and the left frontal cortex. Seed-based correlation maps were formed by computing the normalized Pearson correlation coefficient between the average signal of those two seeds and each individual voxel of the dataset. R

Secondly, using the ultrasensitive Doppler volume, the acquisitions were manually registered (rigid transformation) using known vascular landmarks to two brain atlases: the Papp atlas for subcortical structures[24] and Valdes-Hernandez atlas for cortical structures[25]. Structure labels were subsequently hierarchized using the Neuronames ontology[26] to group them in six larger regions (neocortex, olfactory bulb, midbrain, interbrain). Corresponding brain regions for each number label (103 in total) are listed in Table 2.The spatially averaged and temporally filtered signals were extracted from each of the base regions of interest, normalized and correlated with each other to form the correlation matrix using the MATLAB software. A mean correlation matrix (N_{rats}=4) reflecting inter-regional connectivity is presented in Fig. 2b (individual matrices presented in Supplementary Fig. 1). We chose to measure the 3D functional connectivity in 4 rats to prove the robustness of our modality to detect functional patterns and to minimize the numbers of used animals.

A visual representation of the brain connectivity networks was constructed from the connectivity matrix by creating color-coded plots using the Pearson correlation value and linking the barycenter of each region of interest in three dimensions.

Induction of epileptiform events

Epileptiform ictal events were induced by the cortical injection of 1 μl of 4-aminopyridine (4-AP; Sigma-Aldrich) solution at a concentration of 15 mmol/l using a 150-μm-diameter Hamilton needle, 1 mm deep into the cortex of the anesthetized animal with continuous injections of medetomidine (Domitor®, 0.1 $mg.kg^{-1}.hr^{-1}$) and ketamine (Imalgene®, $12.5mg.kg^{-1}.hr^{-1}$).

It should be noted that our 4AP injection model was not designed to provide new insights into seizure dynamics as such events are distinct from the spreading depressions we tracked in our experiments.

In this set of experiments, a MP 8-angles transmit sequence (390-Hz PRF, for 350 ms, 136 compounded volumes) repeated every 3 s during 360 seconds was used to follow the crisis propagation.

As we were able to detect the propagation of spreading depression waves in 2 rats, we didn't use more animals for this proof of concept in order to minimize the number of used animals.

Supplementary Material

Refer to Web version on PubMed Central for supplementary material.

Acknowledgments

This work was supported by the European Research Council under the European Union's Seventh Framework Program (FP7/2007-2013) / ERC Advanced grant agreement n° 339244-FUSIMAGINE) and by a funding from the Human Brain Project, Projet FUSIMICE ANR-15-HBPR-0004. This work was also supported by the AXA Research Fund.

References

1. Friston KJ. Modalities, Modes, and Models in Functional Neuroimaging. Science. 2009; 326:399–403. [PubMed: 19833961]
2. Xia, Jun; Wang, LV. Small-Animal Whole-Body Photoacoustic Tomography: A Review. IEEE Transactions on Biomedical Engineering. 2014; 61:1380–1389. [PubMed: 24108456]
3. Razansky D, Buehler A, Ntziachristos V. Volumetric real-time multispectral optoacoustic tomography of biomarkers. Nature Protocols. 2011; 6:1121–1129. [PubMed: 21738125]
4. Gottschalk S, Felix Fehm T, Luís Deán-Ben X, Razansky D. Noninvasive Real-Time Visualization of Multiple Cerebral Hemodynamic Parameters in Whole Mouse Brains Using Five-Dimensional Optoacoustic Tomography. J Cereb Blood Flow Metab. 2015; 35:531–535. [PubMed: 25586142]
5. Macé E, et al. Functional ultrasound imaging of the brain. Nature Methods. 2011; 8:662–664. [PubMed: 21725300]
6. Mace E, et al. Functional ultrasound imaging of the brain: theory and basic principles. IEEE Transactions on Ultrasonics, Ferroelectrics and Frequency Control. 2013; 60:492–506.
7. Deffieux T, Demene C, Pernot M, Tanter M. Functional ultrasound neuroimaging: a review of the preclinical and clinical state of the art. Current Opinion in Neurobiology. 2018; 50:128–135. [PubMed: 29477979]
8. Tanter M, Fink M. Ultrafast imaging in biomedical ultrasound. IEEE transactions on ultrasonics, ferroelectrics, and frequency control. 2014; 61:102–119.
9. Tiran E, et al. Multiplane wave imaging increases signal-to-noise ratio in ultrafast ultrasound imaging. Physics in Medicine and Biology. 2015; 60:8549–8566. [PubMed: 26487501]

10. Errico C, et al. Transcranial functional ultrasound imaging of the brain using microbubble-enhanced ultrasensitive Doppler. NeuroImage. 2016; 124:752–761. [PubMed: 26416649]
11. Osmanski B-F, Pezet S, Ricobaraza A, Lenkei Z, Tanter M. Functional ultrasound imaging of intrinsic connectivity in the living rat brain with high spatiotemporal resolution. Nature Communications. 2014; 5
12. De Luca M, Beckmann CF, De Stefano N, Matthews PM, Smith SM. fMRI resting state networks define distinct modes of long-distance interactions in the human brain. NeuroImage. 2006; 29:1359–1367. [PubMed: 16260155]
13. van den Heuvel MP, Hulshoff Pol HE. Exploring the brain network: A review on resting-state fMRI functional connectivity. European Neuropsychopharmacology. 2010; 20:519–534. [PubMed: 20471808]
14. Ayata C, Lauritzen M. Spreading Depression, Spreading Depolarizations, and the Cerebral Vasculature. Physiological Reviews. 2015; 95:953–993. [PubMed: 26133935]
15. Cain SM, et al. In vivo imaging reveals that pregabalin inhibits cortical spreading depression and propagation to subcortical brain structures. Proc Natl Acad Sci U S A. 2017; 114:2401–2406. [PubMed: 28223480]
16. Dizeux A, et al. Functional ultrasound imaging of the brain reveals propagation of task-related brain activity in behaving primates. Nature Communications. 2019; 10
17. Bourdeau RW, et al. Acoustic reporter genes for noninvasive imaging of microorganisms in mammalian hosts. Nature. 2018; 553:86–90. [PubMed: 29300010]
18. Sieu L-A, et al. EEG and functional ultrasound imaging in mobile rats. Nature Methods. 2015; 12:831–834. [PubMed: 26237228]
19. Demene C, et al. Functional ultrasound imaging of brain activity in human newborns. Science translational medicine. 2017; 9:eaah6756. [PubMed: 29021168]
20. Provost J, et al. 3D ultrafast ultrasound imaging in vivo. Phys Med Biol. 2014; 59:L1. [PubMed: 25207828]
21. Bercoff J, et al. Ultrafast compound Doppler imaging: providing full blood flow characterization. IEEE Trans Ultrason Ferroelectr Freq Control. 2011; 58:134–147. [PubMed: 21244981]
22. Demene C, et al. Spatiotemporal Clutter Filtering of Ultrafast Ultrasound Data Highly Increases Doppler and fUltrasound Sensitivity. IEEE Transactions on Medical Imaging. 2015; 34:2271–2285. [PubMed: 25955583]
23. Demené C, et al. 4D microvascular imaging based on ultrafast Doppler tomography. NeuroImage. 2016; 127:472–483. [PubMed: 26555279]
24. Papp EA, Leergaard TB, Calabrese E, Johnson GA, Bjaalie JG. Waxholm Space atlas of the Sprague Dawley rat brain. NeuroImage. 2014; 97:374–386. [PubMed: 24726336]
25. Hernandez V, et al. An in vivo MRI Template Set for Morphometry, Tissue Segmentation, and fMRI Localization in Rats. Front Neuroinform. 2011; 5
26. Bowden DM, Song E, Kosheleva J, Dubach MF. NeuroNames: An Ontology for the BrainInfo Portal to Neuroscience on the Web. Neuroinform. 2012; 10:97–114.

Europe PMC Funders Author Manuscripts

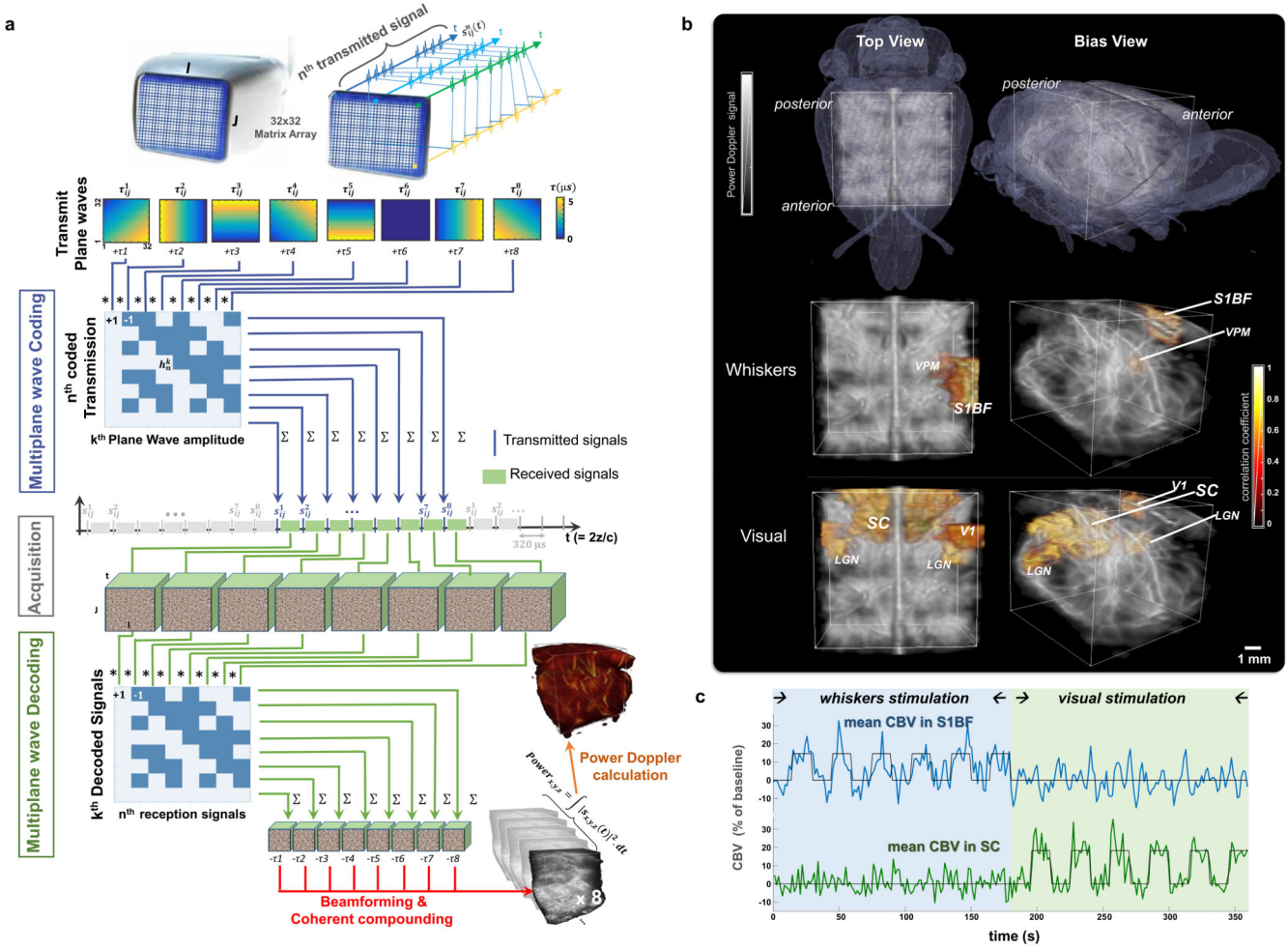

Figure 1. 4D functional ultrasound imaging during task evoked activations

a) Schematic representation of multiplane wave compounding method, with 8 plane waves. At transmit signal #1, 8 wavefronts tilted with 8 different angles are quasi simultaneously transmitted into the medium. This transmit is repeated 8 times with different polarizations +1 or −1 given by the Hadamard matrix H_8. Those coefficients are then used as combination for subtraction or addition operations to retrieve each plane wave individually with an amplitude N. The amplitude increases by coherent summation results in an improvement of the signal-to-noise ratio of the image. b) Example of activation maps (top views and bias views) obtained with the same rat after left whiskers stimulation and visual stimulation respectively. Gray color represents the baseline Doppler signal and activated regions are represented in hot colors. Activation maps were obtained by estimating the Pearson correlation coefficient between the power Doppler signal and the stimulus pattern. Color scale is proportional to the correlation coefficient. Activated ROIs: Somatosensory barrel field (S1BF): r=0.68, and Ventral Posterior Medial Nucleus (VPM): r=0.58 during Whiskers Stimulation, and Primary Visual Cortex (V1): r=0.23, Superior Colliculus (SC): r=0.91, and Lateral Geniculate Nucleus (LGN): r=0.82 during Visual Stimulation. C) Normalized mean CBV signal over responding pixels in the responding areas during the two stimulation

Europe PMC Funders Author Manuscripts

periods. From top to bottom: blue curve= mean CBV signal in S1BF; green curve= mean CBV signal in SC.

Europe PMC Funders Author Manuscripts

Europe PMC Funders Author Manuscripts

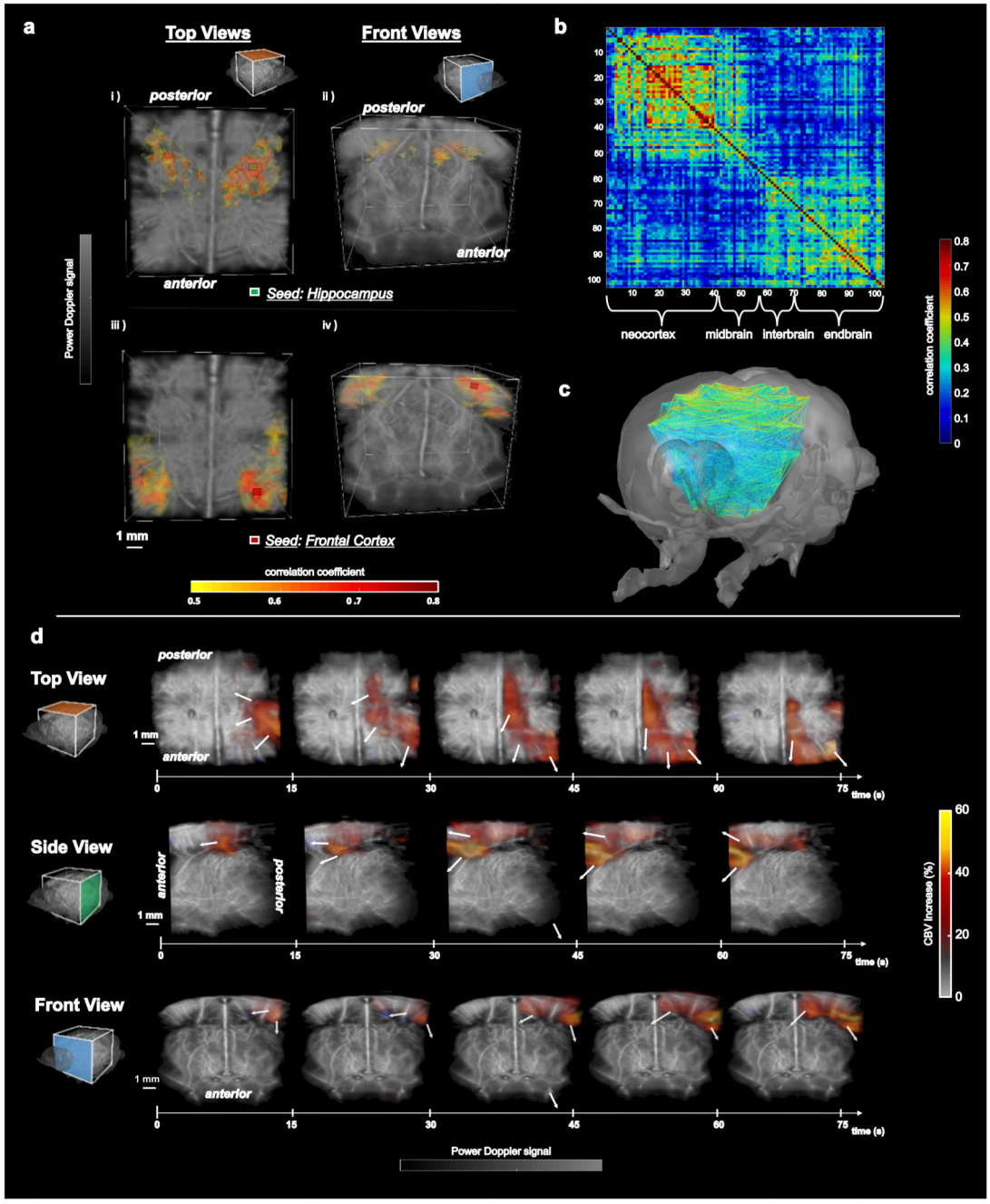

Figure 2. Application of whole rat brain fUS imaging to functional connectivity mapping and 4D tracking of epileptiform events

a) Example of 3D correlation maps obtained in one rat with seed-based analyses. Gray color represents the baseline Doppler signal and regions which exhibit significant correlation with seeds are displayed in hot colors. Seed positioned within left hippocampus (green square): i) top view and ii) coronal view. Seed positioned within frontal cortex (red square): iii) top view and iv) coronal view. Correlation maps were obtained by computing the normalized Pearson correlation coefficient between the temporal signals of each studied seed and each voxel of the brain b) Mean (N_rats=4) correlation matrix of 103 cortical and subcortical

regions. c) Average connectivity graph (correlation coeff. > 0.6 between two linked regions) illustrating 70 connections during resting-state. The color scale represents the strength of functional connections. d) Three views of propagation of a cortical depression wave in a single rat during an ictal event induced by a cortical injection of a potassium channel blocker (4-AP). Power Doppler blood volume increases between 15% and 50% during ictal activity. Wave traveling speed =3 ± 0.3 mm/min.

Europe PMC Funders Author Manuscripts

Europe PMC Funders Author Manuscripts

Table 1

Coordinates of the virtual sources emitting the multiplane waves, and corresponding angle measurements in both planes of the insonified medium (for planes (z,x) and (z,y) see Supplementary Fig. 5)

Source n°	X_{source}	Y_{source}	Angle in (z,x)	Angle in (z,y)
1	2	-2	2.13°	-1.01°
2	-2	2	-2.13°	1.91°
3	1	-1	1.12°	-1.01°
4	-1	1	-1.12°	1.01°
5	2	0	2.13°	0°
6	-1	0	-1.12°	0°
7	0	1	0°	1.01°
8	0	-1	0°	-1.01°